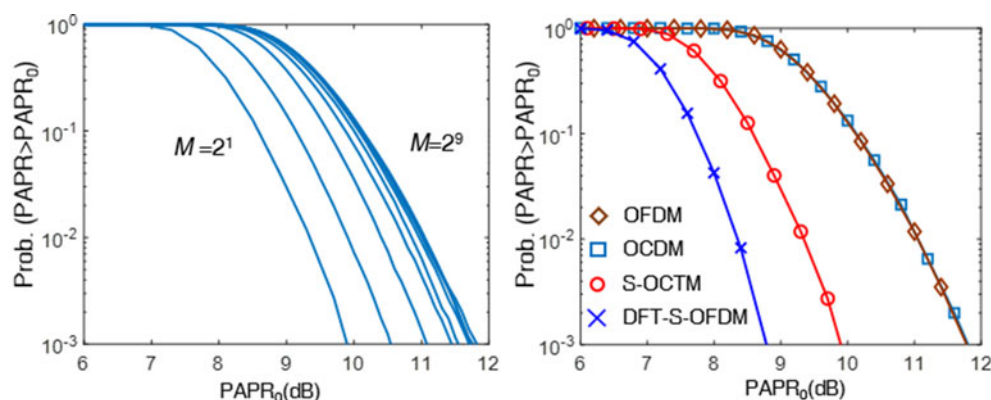| Title	Sparse orthogonal circulant transform multiplexing for coherent optical fiber communication
Authors	Yu, Yukui;Wang, Wei;Ouyang, Xing;Wang, Zhenpeng;Zhao, Jian
Publication date	2018-01-23
Original Citation	Yu, Y., Wang, W., Ouyang, X., Wang, Z. and Zhao, J. (2018) 'Sparse Orthogonal Circulant Transform Multiplexing for Coherent Optical Fiber Communication', IEEE Photonics Journal, 10(1), pp. 1-14.
Type of publication	Article (peer-reviewed)
Link to publisher's version	10.1109/JPHOT.2018.2796846
Rights	© 2018 IEEE. Personal use of this material is permitted. Permission from IEEE must be obtained for all other uses, in any current or future media, including reprinting/republishing this material for advertising or promotional purposes, creating new collective works, for resale or redistribution to servers or lists, or reuse of any copyrighted component of this work in other works.
Download date	2024-06-07 18:58:13
Item downloaded from	https://hdl.handle.net/10468/5473

Open Access

Sparse Orthogonal Circulant Transform Multiplexing for Coherent Optical Fiber Communication

Yukui Yu
Wei Wang
Xing Ouyang
Zhenpeng Wang
Jian Zhao

(a) PAPR performance of S-OCTM schemes with M = 2^m, where m varied from 1 to 9 and (b) PAPR performance of various schemes. The subcarrier number is 1024 and the 16-QAM was used.

IEEE

Sparse Orthogonal Circulant Transform Multiplexing for Coherent Optical Fiber Communication

Yukui Yu [1,2] **Wei Wang,** [1] **Xing Ouyang,** [2] **Zhenpeng Wang,** [1] **and Jian Zhao** [2]

[1] College of Automation, Harbin Engineering University, Harbin 150001, China
[2] Photonic Systems Group, Tyndall National Institute and University College Cork, Cork T12 R5CP, Ireland

Abstract: This paper introduces a new multicarrier system, named sparse orthogonal circulant transform multiplexing (S-OCTM), for optical fiber communication. This technique uses an inverse sparse orthogonal circulant transform (S-OCT) matrix, which is simple and contains only two nonzero elements in each column, to multiplex information of different subcarriers. We compared the proposed scheme with conventional orthogonal frequency division multiplexing (OFDM), orthogonal chirp division multiplexing (OCDM), and discrete-Fourier-transform spreading OFDM (DFT-S-OFDM) in a coherent optical communication system. It is shown that S-OCTM, while exhibiting the complexity among the least, avoids the performance disadvantages of all investigated conventional schemes. It is theoretically proved that the S-OCT matrix equalizes the bandwidth limitation effect that degrades the performance of conventional OFDM. It also shows a greatly reduced peak-to-average power ratio and higher tolerance to fiber nonlinearity than OFDM and OCDM. On the other hand, compared to DFT-S-OFDM, S-OCTM shows a better dispersion tolerance under insufficient length of cyclic prefix and is more tolerable to strong optical filtering. The performance advantages and low complexity enable the proposed scheme to be a promising multicarrier solution for optical communications.

Index Terms: Fiber optics communications, modulation, orthogonal frequency division multiplexing (OFDM).

1. Introduction

Orthogonal frequency division multiplexing (OFDM) has been proven to be a viable technique for optical communication, in favor of its flexible data rate and simple compensation of inter-symbol interference (ISI) caused by the chromatic dispersion (CD) and the polarization mode dispersion (PMD) in optic fibers [1]–[3]. These features are also critical for future generation agile software-defined optical networks with finer data rate granularity. However, OFDM suffers from a high peak-to-average power ratio (PAPR) and the bandwidth limitation effect.

Various designs of pre-emphasis and adaptive loading have been reported to deal with the bandwidth limitation effect [4], but they require prior knowledge of the frequency response and incur higher complexity. Alternatively, spreading OFDM [5]–[11] inherits the advantages of OFDM, and additionally can be more tolerable to the channel fading effect. The fading equalization is achieved by spreading the information over all subcarriers with a spreading/precoding transform and so a flat signal-to-noise ratio (SNR) is obtained over the entire bandwidth. However, the precoding and inverse precoding operation at the transceivers increase the computational complexity, especially when the spreading matrix elements are complex-valued. In addition, some conventional spreading OFDM schemes, such as orthogonal circulant matrix transform (OCT) spreading [6], [7] etc., remain the drawback of a high PAPR. Discrete Fourier transform spreading OFDM (DFT-S-OFDM) can suppress the PAPR [8], [9]. However, similar to a single-carrier format, DFT-S-OFDM is sensitive to the ISI and so shows degraded performance when the length of cyclic prefix (CP) is not sufficient.

Rather than the spreading OFDM structure, orthogonal chirp division multiplexing (OCDM) scheme [10], [11], which uses the discrete Fresnel transform (DFnT) for multicarrier communications, was recently proposed. By spreading information over both temporal and frequency dimensions, this scheme can have higher tolerance to the bandwidth limitation effect than OFDM and more robustness to ISI than DFT-S-OFDM. However, this scheme still suffers from high PAPR due to the superposition of many independent individual chirps, as well as some additional implementation complexity.

In this paper, we propose a low-complexity sparse orthogonal circulant matrix transform multiplexing (S-OCTM) system which avoids the disadvantages of aforementioned schemes, and is robust to both linear (the bandwidth limitation effect and ISI) and nonlinear impairment (PAPR and fiber nonlinearity). In the proposed S-OCTM scheme, the inverse sparse orthogonal circulant matrix transform (I-S-OCT) and S-OCT are used to multiplex/demultiplex the subcarriers. The S-OCT matrix is both unitary and circulant, but with most elements being zeros. A complexity analysis and comparison of S-OCTM, DFT-S-OFDM, OCDM and OFDM are provided, showing that the proposed scheme has the same number of complex multiplications as OFDM and DFT-S-OFDM, much lower than OCDM. Moreover, the proposed scheme owns a lower PAPR performance than both OCDM and OFDM, and consequently a better nonlinearity performance. The mathematical expression for the SNR and the BER of S-OCTM is derived, which, together with numerical simulations, indicates that S-OCTM can equalizes the bandwidth limitation effect and achieves a significant BER improvement over OFDM. We also show that S-OCTM is less sensitive to ISI and so exhibits better performance than DFT-S-OFDM when the length of CP is not sufficient. Finally, we investigate a wavelength division multiplexing (WDM) system with cascaded wavelength selective switches (WSSs), and the results show S-OCTM also owns the best performance in the presence of strong optical filtering. Therefore, the proposed scheme is a promising multicarrier solution for optical communications.

2. Principle

2.1 Proposed S-OCT Transform

Discrete time sequence $\mathbf{c} = [c_1, c_2 \ldots, c_M]^T$, such as the binary and quadri-phase sequences [12], the Frank-Zadoff-Chu (FZC) sequence [13], [14] and the generalized chirp-like sequence [15] etc., with periodic autocorrelation function being a delta function, is usually called perfect or ideal sequence, where $(\bullet)^T$ denotes the transpose operator and $M > 1$. The M-by-M OCT matrix $\mathbf{C}$ takes the form of a circulant of the perfect sequence, $\mathbf{C} = \text{circ}\,[\mathbf{c}]$, which can be easily proved to be both circulant and unitary. However, because the largest length of the perfect sequence $\mathbf{c}$ is limited, for example the perfect binary sequences of length $M > 4$ is unknown [16], or the elements of $\mathbf{c}$ is complex-valued, the OCT matrix $\mathbf{C}$ of large size is not feasible and/or introduces a high implemental complexity.

In this paper, we propose an N-by-N S-OCT matrix $\mathbf{W}$ in the form of $\mathbf{W} = \text{circ}\,[\mathbf{w}]$, and $\mathbf{w}$ is defined as,

$$\mathbf{w} = [w_1, w_2, \ldots, w_N]^T = [c_1, \underbrace{0, 0, \ldots, 0}_{L-1}, c_2, \underbrace{0, 0, \ldots, 0}_{L-1}, \ldots, c_M, \underbrace{0, 0, \ldots, 0}_{L-1}]^T \quad (1)$$
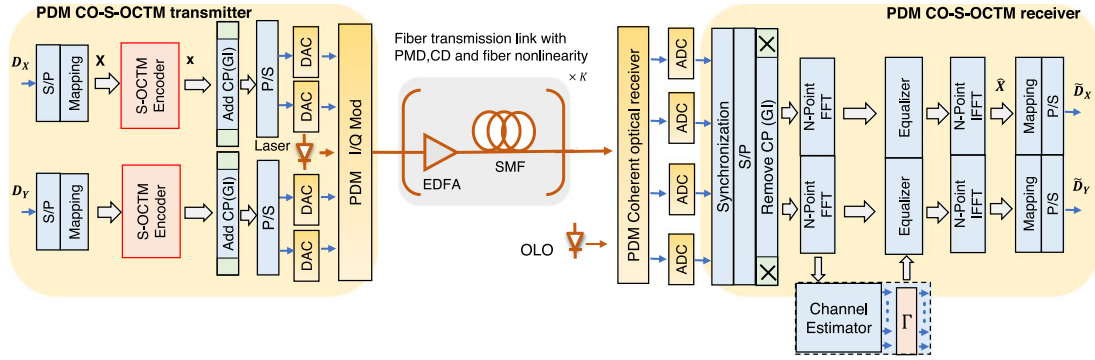
Fig. 1. Schematic of the PDM S-OCTM system architecture. EDFA: erbium doped fiber amplifier; S/P: serial to parallel conversion; P/S: parallel to serial conversion; ADC: analog to digital converter; DAC: digital to analog converter; SMF: single mode fiber; OLO: optical local oscillator.

where $N = L \times M$, and L is integer greater than 1.

It can be easily proved that $\mathbf{WW}^H = \mathbf{I}$, thus $\mathbf{W}$ is both unitary and circulant, the same as the OCT matrix $\mathbf{C}$. By changing L, the size of $\mathbf{W}$ is no longer limited by the largest length of the perfect sequence $\mathbf{c}$ and thus is feasible. Moreover, compared to traditional N-by-N OCT matrix $\mathbf{C}$, because most elements in $\mathbf{W}$ are zeros, the number of complex-valued non-zero elements in $\mathbf{W}$ is reduced remarkably, thus the implementation complexity of S-OCT matrix $\mathbf{W}$ is lower than that of traditional N-by-N OCT matrix $\mathbf{C}$.

To further reduce the computational complexity of $\mathbf{W}$ for practical applications, we can constrain the non-zero elements in each column of $\mathbf{W}$ to the set $\{\pm 1, \pm 1j, (1 \pm 1j)/\sqrt{2}, -(1 \pm 1j)/\sqrt{2}\}$, where $j = \sqrt{-1}$. Then, the operation of multiplying $\mathbf{W}$ can be realized in a simple way. For example, for $M = 4$, only four base sequences $\mathbf{c}$ [12] can be used to construct $\mathbf{W}$: $\mathbf{c} = [1, \varphi, 1, -\varphi]^T$, where $\varphi \in \{1, 1j, (1+1j)/\sqrt{2}, (1-1j)/\sqrt{2}\}$. We can find that the sequence $[1, 1, 1, -1]^T$ is the well-known unique perfect binary sequence with $M = 4$. Please note that the sequences obtained by cyclically shifting and/or multiplying a coefficient are not considered to be a different one from $\mathbf{c}$.

Since most of the elements in $\mathbf{W}$ are zeros, the signal superposition is low when $\mathbf{W}$ is used for coding, resulting in a low PAPR. In this paper, in order to decrease the signal superposition as far as possible, we adopt the perfect sequence $\mathbf{c}$ with $M = 2$ [12]: the perfect quadri-phase sequence $\mathbf{c} = [1, \pm 1j]^T$. No other perfect sequences exist for the length of 2. In this paper, $\mathbf{c} = [1, -1j]^T$ is implied to construct $\mathbf{W}$. Later, the upper bound of the PAPR for the S-OCDM system with different value of M is derived to show the PAPR benefits of the system with $M = 2$.

2.2 Proposed S-OCTM Scheme

In this paper, we use a polarization-division-multiplexed (PDM) coherent optical system to validate the proposed scheme. However, the concept revealed from this study can also be extended to other applications. The block diagram of the PDM CO-S-OCTM system is illustrated in Fig. 1, where it can be seen that, the data symbol vector $\mathbf{X} = [X_0, X_1, \ldots X_{N-1}]^T$ at the transmitter end, is encoded by the N-by-N I-S-OCT matrix $\mathbf{W}^H$. Then, the time-domain signal, $\mathbf{x}$, is,

$$\mathbf{x} = \mathbf{W}^H\mathbf{X} \qquad (2)$$

Similar to the OCT-spreading-OFDM and OCDM, in the S-OCTM, information is spread over both temporal and frequency dimensions, and thus it can be expected that the proposed S-OCTM is more resilient against the bandwidth limitation effect than OFDM and against the ISI effect than DFT-S-OFDM.

Furthermore, as there are only M non-zeros elements in each column of $\mathbf{W}^H$, far fewer than that in the inverse DFnT (IDFnT) matrix in OCDM and the inverse DFT (IDFT) matrix in OFDM, the
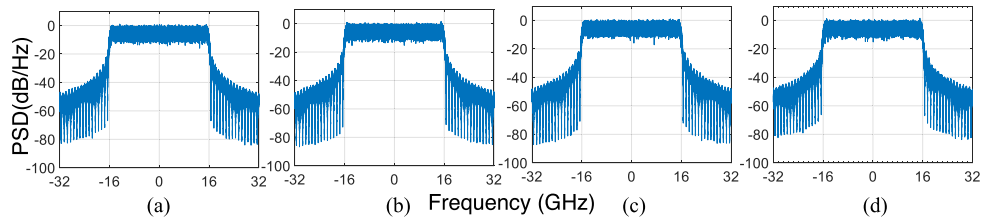
Fig. 2. Power spectral densities of (a) S-OCTM, (b) DFT-S-OFDM, (c) OCDM and (d) OFDM under: the subcarriers number of 1024, 16-QAM mapping, and a symbol rate of 32 Gbaud.

signal superposition is reduced. Thus, the PAPR of the time-domain signal is much less than that in OCDM and OFDM. Moreover, due to the non-zeros elements in $\mathbf{W}$ belong to the set $\{1, -1\mathrm{j}\}$, the encoding operation does not require any complex multiplications, reducing the complexity of the transmitter significantly. A detailed analysis of computational complexity will be discussed later. Also, as shown in Fig. 2, the proposed scheme S-OCTM has the same power spectral density (PSD) as OFDM, DFT-S-OFDM and OCDM.

After adding the CP to eliminate the ISI, the time-domain signal is modulated by I/Q optical modulation and launched into the fiber. It will experience impairments, such as the chromatic dispersion (CD), polarization mode dispersion (PMD) and amplified spontaneous emission (ASE) noise along the fiber link. After removing the CP at the coherent receiver end, the received signal has the form

$$\mathbf{y} = \mathbf{Hx} + \mathbf{n} = \mathbf{HW}^{\mathrm{H}}\mathbf{X} + \mathbf{n} \tag{3}$$

where $\mathbf{H}$ is the channel impulse response matrix, $\mathbf{n}$ is the size-N additive white Gaussian noise vector with a variance of N_0.

By performing the DFT operation on both side of (3), the frequency domain signal can be obtained,

$$\mathbf{y}' = \mathbf{FHx} + \mathbf{Fn} = \mathbf{FHW}^{\mathrm{H}}\mathbf{X} + \mathbf{n}' \tag{4}$$

where $\mathbf{F}$ is the DFT matrix.

We then apply the well-known eigen-decomposition property of a circulant matrix on $\mathbf{W}^{\mathrm{H}}$, i.e., $\mathbf{W}^{\mathrm{H}} = \mathbf{F}^{\mathrm{H}}\Gamma^{\mathrm{H}}\mathbf{F}$, where $\Gamma = \mathrm{diag}\left(\mathbf{F}\left([w_1, w_2 \ldots, w_N]^{\mathrm{T}}\right)\right)$, (4) can be further given by

$$\mathbf{y}' = \mathbf{FHF}^{\mathrm{H}}\mathbf{FW}^{\mathrm{H}}\mathbf{F}^{\mathrm{H}}\mathbf{FX} + \mathbf{Fn} = \Lambda\Gamma^{\mathrm{H}}\mathbf{FX} + \mathbf{n}' \tag{5}$$

where $\mathbf{H} = \mathbf{F}^{\mathrm{H}}\Lambda\mathbf{F}$ with Λ being an N-by-N diagonal matrix with its k-th diagonal element to be the channel frequency response of the k-th subcarrier of interest. It can be observed that, based on the eigen decomposition property, (5) avoids the multiplication of $\mathbf{W}^{\mathrm{H}}$ in (4) by simply combining Γ with diagonal channel frequency response matrix Λ.

In this paper, to compensate the channel effects, a zero-forcing (ZF) equalizer $\mathbf{G} = \Lambda^{-1}$ is adopted. After performing the IDFT operation on the equalized signal, the recovered signal can be expressed as,

$$\hat{\mathbf{X}} = \mathbf{F}^{\mathrm{H}}\Gamma\mathbf{Gy}' = \mathbf{F}^{\mathrm{H}}\Gamma\mathbf{GFy} \tag{6}$$

As shown in the receiver in Fig. 1, the multiplication of Λ can be combined with the single-tap equalization and hence the receiver does not require any additional complex multiplication per symbol.

2.3 Analysis of BER Performance

Due to the bandwidth-limited components such as digital-to-analog convertors (DACs), analog-to-digital convertors (ADCs) and filters etc. in the transceiver, the transmission channel exhibits a low pass filtering property. In this subsection, without the loss of generality, we evaluated the theoretical BER performance of the proposed S-OCTM scheme using 16-QAM data mapping to show its

performance advantage in fading channels. By averaging the BER of the individual subcarriers [16], we can obtain the overall BER as follows:

$$P_e = \frac{3}{4N} \sum_{k=0}^{N-1} Q\left(\sqrt{\frac{SNR_k}{5}}\right) \tag{7}$$

where $Q(x)$ denotes the Q-function of x, and SNR_k represents the SNR of the k-th subcarrier.

For the proposed S-OCTM scheme, based on (6), the k-th element of $\hat{\mathbf{X}}$ can be further written as

$$\hat{X}_k = \underbrace{X_k}_{\mu_{ZF,k}} + \underbrace{\mathbf{F}_k^H \mathbf{G}\mathbf{\Gamma}\mathbf{n}'}_{\delta_{ZF,k}} \tag{8}$$

where $\mu_{ZF,k}$ and $\delta_{ZF,k}$ are the desired signal and the noise of the k-th subcarrier, respectively, and $\mathbf{F}_k$ denotes the k-th column of $\mathbf{F}$. Then, the SNR at the receiver can be evaluated as

$$SNR_{S\text{-}OCTM} = \frac{E\left[|\mu_{ZF,k}|^2\right]}{E\left[|\delta_{ZF,k}|^2\right]} = \frac{E_s}{\frac{N_0}{N}\sum_{k=0}^{N-1}|G_k|^2|\Gamma_k|^2} = \frac{E_s}{\frac{N_0}{N}\sum_{k=0}^{N-1}|G_k|^2} \tag{9}$$

where E_s is the signal power per data symbol, $E[\bullet]$ is the expectation operation, Γ_k is the k-th diagonal element of $\mathbf{\Gamma}$, and G_k is the k-th diagonal element of $\mathbf{G}$. Please note that all the diagonal elements of $\mathbf{\Gamma}$ are of an equal and unit magnitude. Equation (9) verifies that S-OCTM can average the channel fading effects over all frequency components and thus a flat SNR profile can be obtained. Therefore, the detrimental performance degradation can be minimized. Substituting (9) to (7), the overall BER of the S-OCTM with the fading channel can be expressed as

$$P_{e,S\text{-}OCTM} = \frac{3}{4}Q\left(\sqrt{\frac{SNR_{S\text{-}OCTM}}{5}}\right) \tag{10}$$

It is noteworthy that the SNR formula in (9) can also describe the performance of DFT-S-OFDM and OCDM, because they can be regarded as two special cases of S-OCTM with $M = 1$ and $M = N$ respectively. Therefore, the theoretical BERs of the OCDM, DFT-S-OFDM and S-OCTM in fading channel are the same:

$$P_{e,OCDM} = P_{e,DFT\text{-}S\text{-}OFDM} = P_{e,S\text{-}OCTM} \tag{11}$$

However, the SNR for the conventional OFDM in fading channel can be given by

$$SNR_{k,OFDM} = \frac{E_s}{N_0|G_k|^2} \tag{12}$$

Thus, the overall BER performance of OFDM is,

$$P_{e,OFDM} = \frac{3}{4N} \sum_{k=0}^{N-1} Q\left(\sqrt{\frac{SNR_{k,OFDM}}{5}}\right) \tag{13}$$

Please note that BER performance of those schemes with other formats, like QPSK, can also be easily derived in a similar way.

2.4 Analysis of Peak-to-Average Power Ratio

The high PAPR is one of the main drawback of multicarrier systems, which arises from the superposition of a large number of subcarriers. A higher PAPR makes the system vulnerable to fiber nonlinearity effects. In general, the PAPR of the discrete-time signal x is defined as,

$$PAPR\{x\} = 10\log_{10}\left(\frac{\max_{0\leq k\leq N}|x_k|^2}{E\left[|x_k|^2\right]}\right) \text{(dB)} \tag{14}$$

TABLE 1
Computational Complexity of Various Systems

	Transmitter		Receiver	
	Num. of Complex Multip.	Num. of Complex Add.	Num. of Complex Multip.	Num. of Complex Add.
OFDM	$N/2 \times \log_2 N$	$N \times \log_2 N$	$N/2 \times \log_2 N + N$	$N \times \log_2 N$
OCDM	$N/2 \times \log_2 N + 2N$	$N \times \log_2 N$	$N \times \log_2 N + N$	$2N \times \log_2 N$
DFT-S-OFDM	0	0	$N \times \log_2 N + N$	$2N \times \log_2 N$
S-OCTM	0	N	$N \times \log_2 N + N$	$2N \times \log_2 N$

Due to only M nonzero elements in each column of $\mathbf{W}$, each output sample in S-OCTM involves the sum of only M symbols. Thus, the PAPR of the proposed S-OCTM system can be upper bounded as

$$PAPR_{S-OCTM} \leq 10 \log_{10} \left(M \times \frac{|x_k|^2_{max}}{E\left[|x_k|^2\right]} \right) (dB) \tag{15}$$

It can be seen that the upper bound of the PAPR for S-OCTM reduces as M being smaller, which will be verified by numerical simulations later. To decrease the signal superposition as far as possible, the value of M should be the smallest. Therefore, we chose $M = 2$ in this paper.

While for the OCDM and OFDM, because all the elements of the IDFT matrix and the IDFnT matrix are complex valued, each output sample in OCDM and OFDM includes N input symbol superposition, thus their PAPR can be upper bounded as,

$$PAPR_{OCDM/OFDM} \leq 10 \log_{10} \left(N \times \frac{|x_k|^2_{max}}{E\left[|x_k|^2\right]} \right) (dB) \tag{16}$$

We can find that the worst case of the PAPR of S-OCTM is much better than that of both OCDM and OFDM. And the relationship can be written as,

$$PAPR_{S-OCTM} \leq \left(PAPR_{OCDM/OFDM} - 10 \log_{10} \left(\frac{N}{M} \right) \right) (dB) \tag{17}$$

It can be seen that the PAPR advantage is expected to be enhanced as the subcarrier number N increases or M decreases. Note that we adopted $M = 2$ to achieve the largest PAPR advantage in this paper.

2.5 Analysis of Computational Complexity

In the conventional OFDM system, the transmitter requires one IDFT operation, while the receiver requires one DFT operation and N complex multiplications to perform channel equalization. The complexity of the OCDM system is given in [14], [15]. Note that the complexity of the receiver #2 in [14], [15] is adopted in Table 1 because it is the most efficient receiver. In DFT-S-OFDM, when all subcarriers are loaded with data, no complexity multiplication and additions are required at the transmitter because the DFT spreading operation can be combined with the IDFT multiplexing operation to form an identity matrix. In this case, DFT-S-OFDM can be regarded as a single carrier formats. However, the frequency equalization is required at the receiver, which involves one DFT and IDFT operation, and one channel equalization operation. It can be seen that the overall
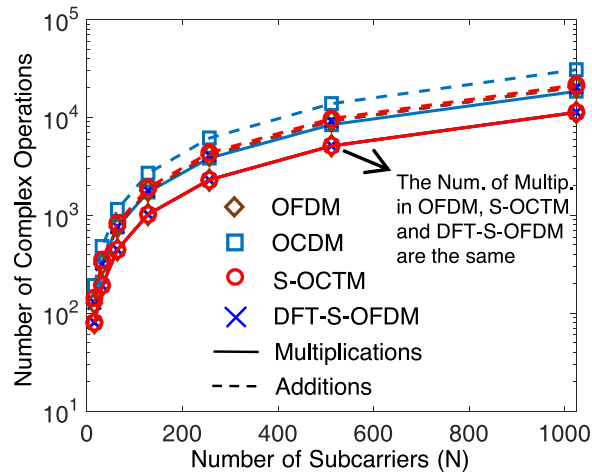
Fig. 3. The number of total complex operations versus the number of subcarriers N.

complexity of DFT-S-OFDM and OFDM are similar. In the proposed S-OCTM system, since each column of the I-S-OCT matrix $\mathbf{W}^H$ contains only two non-zero elements of $\{1, -1j\}$, thus only N complex additions are required at the transmitter. Similar to DFT-S-OFDM, S-OCTM require one IDFT operation, one DFT operation, and one channel equalization at the receiver side. Table 1 summaries the computational complexities of the transmitter and receiver of the OFDM, OCDM, DFT-S-OFDM and S-OCTM. In addition, Fig. 3 depicts the total computational complexity versus the number of subcarriers N. It can be seen that OCDM requires the greatest number of additions and multiplications. It also shows that the S-OCTM, OFDM and DFT-S-OFDM require the same number of complex multiplication, lower than that of OCDM.

3. Simulation Setup and Results

In this section, numerical simulations were carried out to validate the benefits of the proposed S-OCTM over OFDM, OCDM and DFT-S-OFDM. A number of 1024 subcarrier were used. The subcarriers were fully loaded with information, and were encoded with 16-QAM mapping from $2^{23} - 1$ pseudo random bit sequences, with a simulation symbol number of 2^{20}. 6.25% subcarriers were uniformly distributed as the pilots to estimate the laser phase noise by using common phase estimation (CPE) method [17]. The DACs operated at 32-GSample/s and thus the data rate is 256-Gb/s. Raised cosine (RC) filter with a roll-off factor 0.05, unless stated otherwise, was employed to remove the aliasing. Analog signals were generated with an oversampling ratio of 8. The PDM I/Q optical modulator worked at the linear region. The laser operated at 1550 nm. The fiber link consisted of spans of 80-km standard single mode fiber with a dispersion parameter of 16 ps/km/nm, a loss of 0.2 dB/km, a PMD coefficient of 0.1 ps/km$^{1/2}$, and a nonlinear parameter of 1.31/km/W. At the end of each span, an optical amplifier with 16-dB gain and 4.5-dB noise figure was used to compensate the fiber loss. At the receiver, Bessel-type low-pass filters with 3-dB bandwidth of 24 GHz were used before 64-Gsamples/s ADCs. After resampling and synchronization, frequency-domain pilot channel equalization [18] was applied for impairment mitigation and polarization demultiplexing.

3.1 Peak-to-Average Power Ratio

We evaluated the PAPR performance by the complementary cumulative distribution function (CCDF) of the PAPR, which is defined as the probability that the PAPR exceeds a given threshold $PAPR_0$,

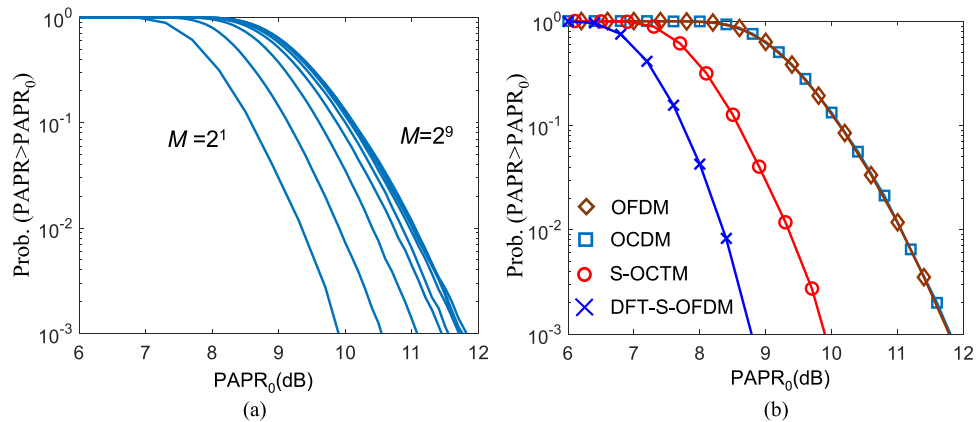$$PAPR = Prob\,(PAPR > PAPR_0) \tag{18}$$

Fig. 4. (a) PAPR performance of S-OCTM schemes with $M = 2^m$, where m varies from 1 to 9 and (b) PAPR performance of various schemes. The subcarrier number is 1024 and the 16-QAM was used.

The simulation adopted an oversampling of 4 to simulate the actual PAPR. The 16-QAM format was used and the subcarrier number was 1024.

We firstly investigated the PAPR performance of S-OCTM with different M, as shown in Fig. 4(a). The value of M is 2^m, where m varied from 1 to 9. It can be seen that the PAPR of S-OCTM increases as M increases, and S-OCTM with $M = 2$ owns the lowest PAPR. We attribute this to the fact that a larger value of M increases the superposition of the subcarriers and results in a higher PAPR, which tightly matches (15).

Then we compared the PAPR performance of various systems in Fig. 4(b). The S-OCTM with $M = 2$ was adopted due to the benefits of PAPR performance as shown in Fig. 4(a). As expected, the PAPR performance of OCDM and OFDM are almost the same in all the cases. However, it can be observed that the proposed S-OCTM systems have a lower PAPR than both OCDM and OFDM, because the sparsity of the S-OCT transform can reduce the superposition of the input symbols. In particular, when $Prob.(PAPR > PAPR_0) = 10^{-3}$, the S-OCTM improves the PAPR performance by almost 1.8 dB. This is also in a good agreement with (17). DFT-S-OFDM is similar to a single carrier format, thus the PAPR performance is the lowest. Compared to the DFT-S-OFDM, the PAPR of S-OCTM is about 1.2 dB higher.

3.2 BER Performance

In this subsection, we neglect fiber nonlinearity effect to investigate the performance sensitivity to ASE noise, dispersion and phase noise. We firstly investigated the BER performance for the back to back case when the raised cosine (RC) aliasing filter had the roll-off factor of (a) 0.05 (b) 0.3, as shown in Fig. 5. The raised cosine filter is employed to emulate the bandlimited signal. The insets (i) and (ii) in Fig. 5 are the transmitted PSD of S-OCTM system when the RC filter has a roll-off factor of 0.05 and 0.3 respectively. Note that all other three formats have the same transmitted PSD with S-OCTM, as shown in Fig. 2. We can find that the signal with a larger roll-off factor RC filter suffers a more severe bandwidth limitation effect. The analytical S-OCTM and OFDM curves in Fig. 5 represent the theoretical calculation of (10) and (13), respectively. It can be seen that the analytical BER curves match the simulation results. As expected, the performance of the S-OCTM, OCDM and DFT-S-OFDM are almost the same, better than that of OFDM. Moreover, due to the more serious bandwidth limitation in Fig. 5(b), the performance of OFDM in Fig. 5(b) is worse than that in Fig. 5(a). On the other hand, the performances of the other three formats are similar in Fig. 5(a) and (b), because they can equalize the bandwidth limitation effect. The raised cosine filter with the roll-off factor 0.05 will be adopted in the following.

Then, the BER performances over the dispersive fiber channel were evaluated. Fig. 6(a) and (b) shows the performance comparisons at the dispersion of 800 km and 1120 km, respectively.
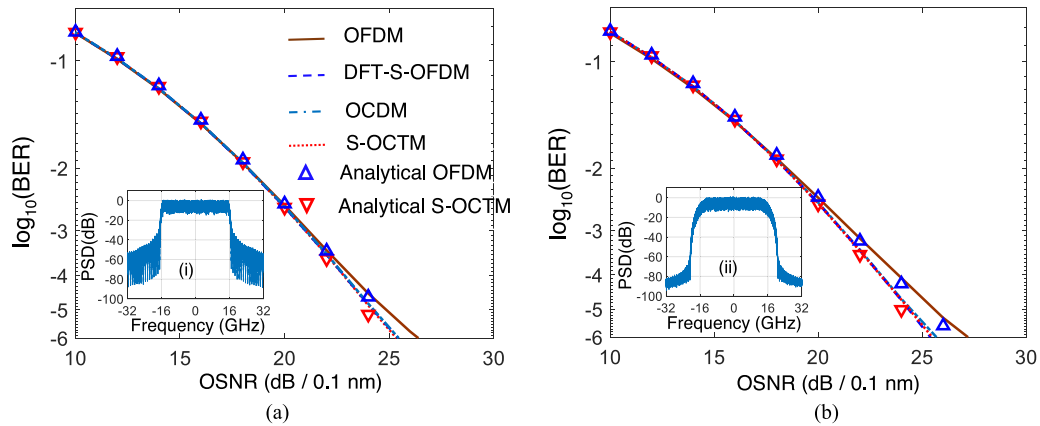
Fig. 5. BER versus OSNR (dB/0.1 nm) for the back to back case when the raised cosine filter has a roll-off factor of (a) 0.05; (b) 0.3. The insets (i) and (ii) are the transmitted spectra of S-OCTM system when the raised cosine filter has a roll-off factor of 0.05 and 0.3 respectively. Laser linewidth is set to be zero. At back-to-back, the main impairment is the bandwidth limitation effect.
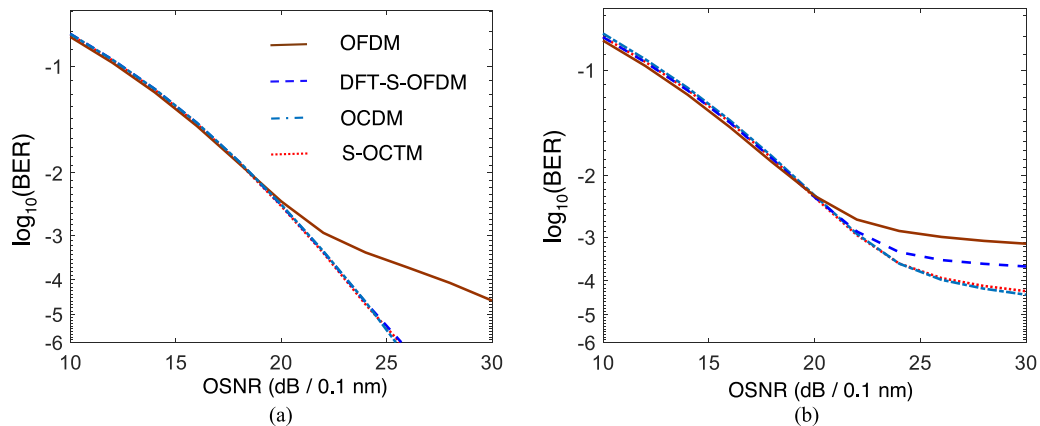

Fig. 6. BER versus OSNR (dB/0.1 nm) at the dispersion of (a) 800 km; (b) 1120 km. The length of CP in (a) is sufficient while in (b) is insufficient. Laser linewidth is set to be zero. Fiber nonlinearity and laser phase noise are not included and the main impairments in this figure are the bandwidth limitation effects, and dispersion.

The CP length of 4 ns was used, which is at the margin to compensate the dispersion of 960 km. This length can be predicted by $T_{CP}/(2\pi\beta_2 f_s)$, where T_{CP}, β_2, f_s are the length of CP, dispersion coefficient, and signal bandwidth, respectively. Therefore, the CP is sufficient in Fig. 6(a) while insufficient in Fig. 6(b). We can find that the performances of the S-OCTM, OCDM and DFT-S-OFDM in Fig. 6(a) are similar to that in Fig. 5(a), while the performance of OFDM is worse in Fig. 6(a) than that in Fig. 5(a). We attribute this to the fact that: in the presence of bandwidth limitation effect and large dispersion, the amplitude and phase of the subcarriers in the high frequencies will vary and the orthogonality of the OFDM subcarriers are destroyed, resulting in a spectral notch in high frequencies. This spectral notch degrades the performance of OFDM remarkably, while other three schemes can average this performance degradation. In Fig. 6(b), all the formats exhibit a performance degradation. The figure shows that the performance of the S-OCTM and OCDM are still similar, better than that of DFT-S-OFDM. This is because that DFT-S-OFDM can be regarded as a single carrier format and thus is more sensitive to the ISI effects. While both S-OCTM and OCDM inherit the dispersion tolerance of the multi-carrier formats.

Finally, we included the laser linewidth and compared the BER performances at the distances of (a) 800-km and (b) 1120-km, as shown in Fig. 7. The laser linewidth is 100-kHz. It can be seen
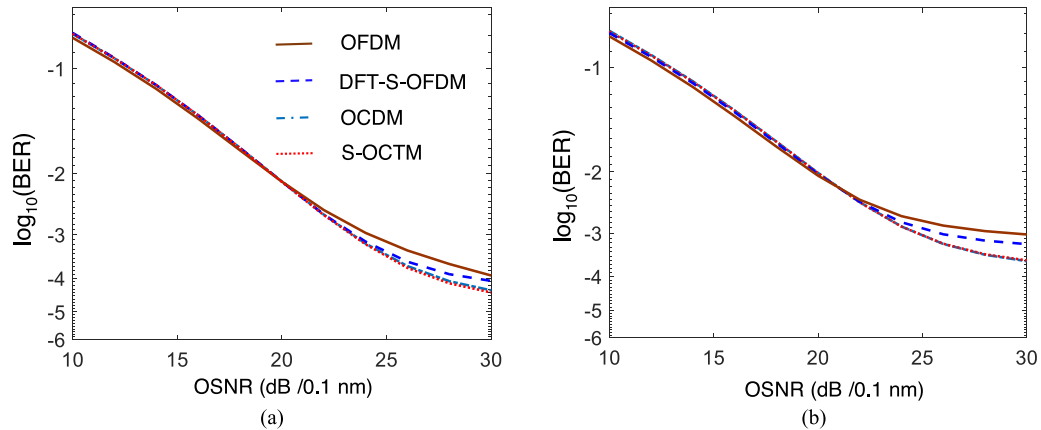
Fig. 7. BER versus OSNR (dB/0.1 nm) at a distance of (a) 800 km; (b) 1120 km. The laser linewidth is 100 kHz. The laser phase noise was estimated by the CPE method. Fiber nonlinearity is not included and the main impairments in this figure include the bandwidth limitation effects, dispersion, and residual laser phase noise.
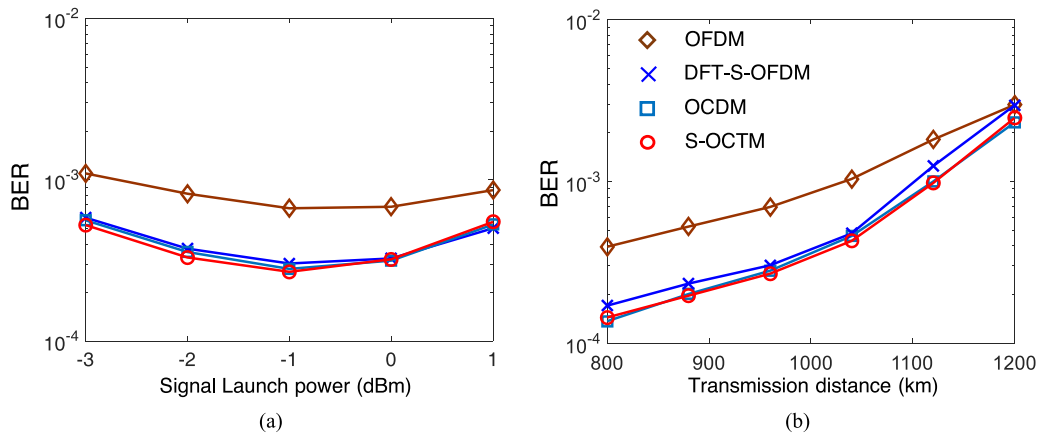

Fig. 8. (a) BER versus the launch power at a transmission distance of 960 km; (b) BER at the optimal signal launch power versus the transmission distances. The laser phase was estimated by the CPE method. The impairments in this figure include both linear (bandwidth limitation effect, dispersion, laser noise as in Fig. 7) and intra-channel nonlinearity.

that the DFT-S-OFDM shows a worse performance than both S-OCTM and OCDM in the high OSNR regions in Fig. 7(a). This is mainly because that DFT-S-OFDM introduces a more severe inter-sub-carrier interference (ICI) than both S-OCTM and OCDM, due to the DFT spreading phase offset mismatch caused by random phase noise. Fig. 7(b) shows that the S-OCTM and OCDM can still outperform DFT-S-OFDM in presence of both the laser linewidth and the ISI.

3.3 Single-Channel Transmission Performance

In this subsection, we included the fiber nonlinearity to evaluate the transmission performance under the 100-kHz laser linewidth in single-channel transmission. Fig. 8(a) shows the BER performance at a transmission distance of 960 km versus the signal launch power. The length of CP is 4 ns. It is shown that the performance of S-OCTM, DFT-S-OFDM and OCDM are similar, all better than that of OFDM. The performance of the OFDM is mainly limited by the bandwidth limitation effects while other three formats can effectively equalize the bandwidth- and dispersion-induced fading,
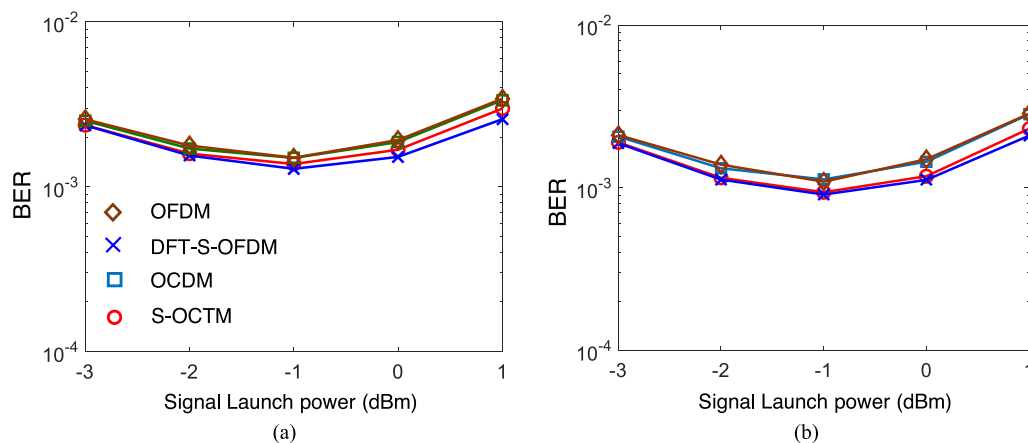
Fig. 9. BER versus the launch power at a transmission distance of 1600 km: (a) the laser phase noise was estimated by the CPE method; (b) the estimation of the laser phase noise was assumed to be perfect. The impairments include bandwidth limitation and nonlinearity while dispersion is ideally compensated. Residual laser phase noise effect is included in (a) and is not included in (b).

because their information is distributed over all the signal spectrum. This is also in good agreement with (9). Fig. 8(b) shows the BER at the optimal signal launch power versus the transmission distances. It can be observed that the S-OCTM, although exhibiting a lower complexity, shows the similar performance with the OCDM for the distances longer than 960-km, namely when the CP is insufficient. This is because the S-OCTM owns a similar dispersion tolerance as the OCDM. While DFT-S-OFDM, which can be viewed as a single-carrier format, is more vulnerable to the ISI effects and so gives more degraded performance when the CP length is not sufficient.

In order to clearly show the nonlinear tolerance of different technologies, we investigate the performance when the dispersion was ideally compensated at the receiver end. An ideal dispersion compensating fiber (DCF), without nonlinearity and loss, was placed at the end of transmission link to combat the dispersion. In practice, this DCF module can also be replaced by frequency-domain electronic dispersion compensation. Fig. 9(a) shows the BER performance versus the signal launch power at a transmission distance of 1600 km. It can be seen that the performance of OFDM approaches to that of OCDM, this is because the roll-off of the raised cosine filter in this paper was small (0.05) and the dispersion was ideally compensated. However, please note that the performance of OFDM will be degraded significantly when the bandwidth limitation effect is severe, as shown in Fig. 5.

Additionally, in Fig. 9(a), in the high launch power region (> -1 dBm), S-OCTM exhibits a slight BER degradation than DFT-S-OFDM, but better than both OCDM and OFDM. This indicates that S-OCTM owns a better nonlinearity tolerance than both OCDM and OFDM, while DFT-S-OFDM gives the best nonlinear tolerance. This matches the PAPR analysis in Fig. 4. In order to demonstrate the nonlinearity tolerance more clearly, we re-investigated the performance comparisons with the assumption of perfect estimation of the laser phase noise, as shown in Fig. 9(b). It can be seen that S-OCTM outperforms both OCDM and OFDM, showing the advantage of nonlinearity robustness, due to a lower PAPR. Fig. 10 depicts the BER performance comparisons at the optimal signal launch power versus the transmission distances. It can be seen that S-OCTM, while giving a higher tolerance to ISI, shows similar nonlinear performance as DFT-S-OFDM, better than both OCDM and OFDM.

3.4 WDM-Channel Transmission Performance

In this subsection, we investigate the performance of WDM systems consisting of seven channels with 50-GHz channel spacing. The ideal DCF was adopted at the receiver end to compensate
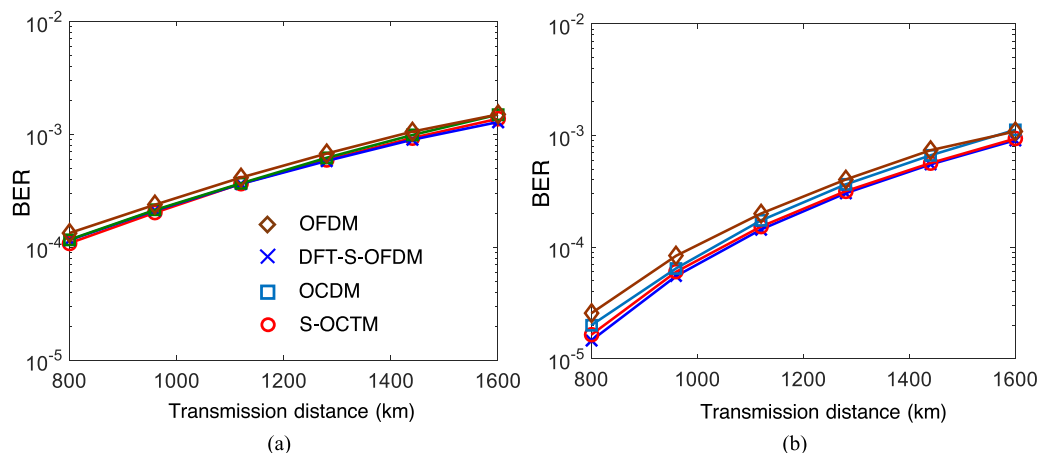
Fig. 10. BER at the optimal signal launch power versus the transmission distances: (a) the laser phase noise was estimated by the CPE method; (b) the estimation of the laser phase noise was assumed to be perfect. The impairments include bandwidth limitation and nonlinearity while dispersion is ideally compensated. Residual laser phase noise effect is included in (a) and is not included in (b).
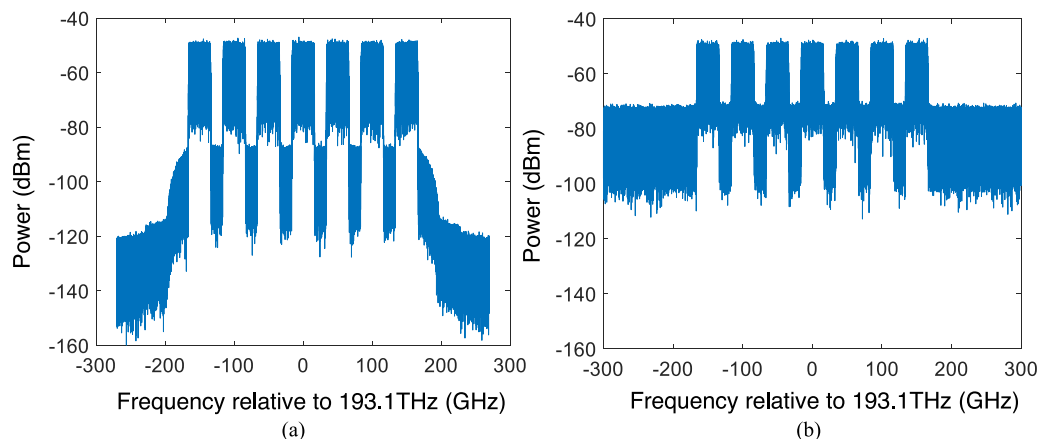

Fig. 11. Simulated optical spectrum of a 50-GHz spaced WDM system with seven PDM CO-S-OCTM wavelength channels. (a) Transmitted optical spectrum and (b) received optical spectrum.

dispersion effects ideally. The laser linewidth was 100-kHz and the phase noise was estimated by CPE method. Fig. 11(a) and (b) shows the optical spectrum of the WDM S-OCTM signal before and after transmission, respectively. Fig. 12(a) shows the BER of the center channel at the optimal signal launch power versus the transmission distances. It is seen that the performance of S-OCTM is similar to that of DFT-S-OFDM and better than that both of OFDM and OCDM. In other words, in the WDM case, S-OCTM still reveals a similar fiber nonlinear tolerance as DFT-S-OFDM, better than both OFDM and OCDM. We further add WSSs to emulate the filtering effects in the add/drop nodes. Fig. 12(b) shows BER of the center channel at the optimal signal launch power versus 3-dB bandwidth of the WSS in the WDM system. The WSS is modelled as in [19] with a variable 3-dB bandwidth and a fixed 6-dB bandwidth of 50-GHz. 24 cascaded WSSs are used to emulate 12 add/drop nodes. The cascaded WSSs were placed before the ideal DCF module to simulate the filtering effects raised from the WSSs along the fiber link. Due to the cascaded WSSs filtering fading, it can be seen that OFDM exhibits the worst performance when WSS 3-dB bandwidth is narrower than 43 GHz. Moreover, we can find that S-OCTM shows a better tolerance to the filtering effect than DFT-S-OFDM, and exhibits the best performance in the presence of strong optical filtering.
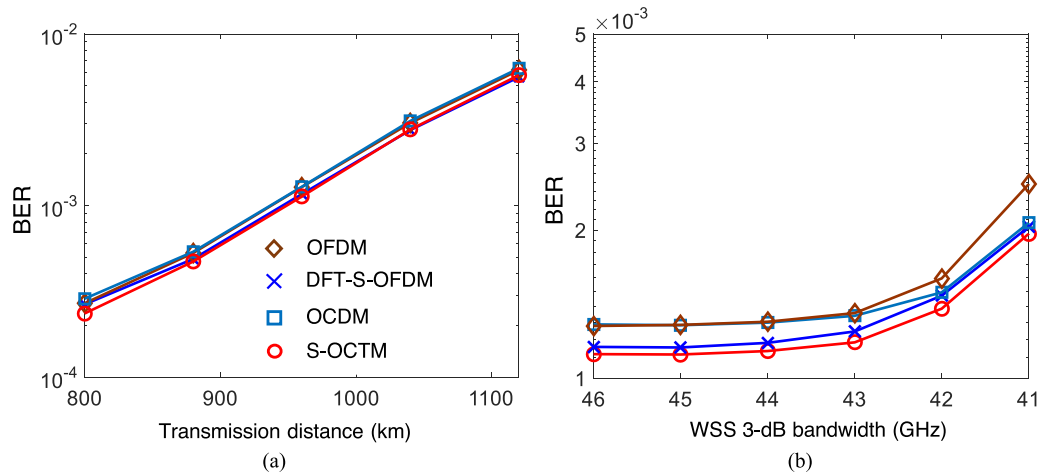
Fig. 12. (a) BER of the center channel of the WDM system versus the transmission distances; (b) BER of the center channel at the optimal signal launch power versus 3-dB bandwidth of the WSS. In (a, b), the number of channels is 7. In (b), the distance is 960 km and 24 cascaded WSS are used to emulated 12 add/drop nodes. The laser phase noise was estimated by CPE method. Both (a) and (b) include the impairments of the bandwidth limitation effects, fiber nonlinearity and the residual laser phase noise. Dispersion is ideally compensated. In (b) cascaded WSSs filtering effect is also included.

TABLE 2

Advantages of S-OCTM Over Other Three Formats Under Multiple Comparison Criteria

	OFDM	DFT-S-OFDM	OCDM
Overall complexity	○	○	△
Bandwidth Limitation	△	○	○
PAPR	△	○	△
Nonlinearity	△	○	△
Robust to the ISI	○	△	○
Strong optical filtering	△	△	○

The circle ○ and triangle △ mark represent a similar and an improvement performance achieved by S-OCTM, respectively.

3.5 Comparison Under Various Criteria

In above subsections, we have investigated the advantages of S-OCTM under multiple comparison criteria: bandwidth limitation effect, PAPR, ISI, and so on. The results are summarized in Table 2. S-OCTM owns a similar computational complexity as DFT-S-OFDM and OFDM, better than OCDM; Similar to OCDM and DFT-S-OFDM, S-OCTM can equalize the bandwidth limitation effect, hence showing a better BER performance than OFDM; S-OCTM results in a much lower PAPR and thus better nonlinear performance than OCDM and OFDM; S-OCDM is more robust to the ISI and strong optical filtering than DFT-S-OFDM. Therefore, S-OCTM avoids the disadvantages of other three schemes, while maintaining the complexity among the least.

4. Summary

We have proposed a novel S-OCTM scheme for optical fiber communication. The S-OCT matrix is constructed by the perfect sequence, with only two non-zero elements are in each column. We have compared the proposed S-OCTM with OFDM, OCDM, and DFT-S-OFDM in terms of both complexity and performance. It is shown that the complexity of S-OCTM is among the least while

it avoids all disadvantages of other schemes: the reduced superposition in S-OCTM results in a much lower PAPR and consequently better nonlinear performance than OCDM and OFDM; Both theoretical derivations and simulations show that S-OCTM can equalize the bandwidth limitation effect that degrades the performance of OFDM; Compared to DFT-S-OFDM, it has been shown that S-OCDM is more robust to the ISI and strong optical filtering in add/drop nodes in the WDM case. The performance advantages and low complexity enable the proposed scheme to be a promising multicarrier solution for optical communications.

References

[1] A. Saljoghei, F. A. Gutierrez, P. Perry, D. Venkitesh, R. D. Koipillai, and L. P. Barry, "Experimental comparison of FBMC and OFDM for multiple access uplink PON," *J. Lightw. Technol.,* vol. 35, no. 9, pp. 1595–1604, May 2017.

[2] J. Zhao, "Channel estimation in DFT-based offset-QAM OFDM systems," *Opt. Exp.,* vol. 22, no. 21, pp. 25651–25662, 2014.

[3] W. Shieh, H. Bao, and Y. Tang, "Coherent optical OFDM: Theory and design," *Opt. Exp.,* vol. 16, no. 2, pp. 841–859, 2008.

[4] R. B. Nunes, A. Shahpari, J. A. L. Silva, M. Lima, P. S. B. Andre, and M. E. V. Segatto, "Experimental demonstration of a 33.5-Gb/s OFDM-based PON with subcarrier pre-emphasis," *IEEE Photon. Technol. Lett.,* vol. 28, no. 8, pp. 860–863, Apr. 2016.

[5] Z. Feng *et al.,* "Dispersion-tolerant DDO-OFDM system and simplified adaptive modulation scheme using CAZAC precoding," *J. Lightw. Technol.,* vol. 34, no. 11, pp. 2743–2751, Jun. 2016.

[6] Y. Yu, W. Wang, X. Ouyang, Z. Wang, and J. Zhao, "Discrete Fresnel transform spread OFDM for coherent optical fiber communication," *IEEE Photon. Technol. Lett.,* vol. 30, no. 1, pp. 91–94, Jan. 2018.

[7] Y. Hong, J. Xu, and L. K. Chen, "Experimental investigation of multi-band OCT precoding for OFDM-based visible light communications," *Opt. Exp.,* vol. 25, no. 11, pp. 12908–12914, 2017.

[8] Y. Wang, J. Yu, and N. Chi, "Demonstration of 4 × 128-Gb/s DFT-S-OFDM signal transmission over 320-km SMF with IM/DD," *IEEE Photon. J.,* vol. 8, no. 2, Apr. 2016, Art. no. 7903209.

[9] F. Li, J. Yu, Y. Fang, Z. Dong, X. Li, and L. Chen, "Demonstration of DFT-spread 256 QAM-OFDM signal transmission with cost-effective directly modulated laser," *Opt. Exp.,* vol. 22, no. 7, pp. 8742–8748, 2014.

[10] X. Ouyang and J. Zhao, "Orthogonal chirp division multiplexing," *IEEE Trans. Commun.,* vol. 64, no. 9, pp. 3946–3957, Sep. 2016.

[11] X. Ouyang and J. Zhao, "Orthogonal chirp division multiplexing for coherent optical fiber communications," *J. Lightw. Technol.,* vol. 34, no. 18, pp. 4376–4386, Sep. 2016.

[12] H. D. Luke, H. D. Schotten, and H. H. Mahram, "Binary and quadriphase sequences with optimal autocorrelation properties: A survey," *IEEE Trans. Inf. Theory,* vol. 49, no. 12, pp. 3271–3284, Dec. 2003.

[13] R. L. Frank and S. A. Zadoff, "Phase shift pulse codes with good periodic correlation properties," *IEEE Trans. Inf. Theory,* vol. 8, no. 6, pp. 381–382, Oct. 1962.

[14] D. Chu, "Polyphase codes with good periodic correlation properties," *IEEE Trans. Inf. Theory,* vol. 18, no. 4, pp. 531–532, Jul. 1972.

[15] B. M. Popovic, "Generalized chirp-like polyphase sequences with optimum correlation properties," *IEEE Trans. Inf. Theory,* vol. 38, no. 4, pp. 1406–1409, Jul. 1992.

[16] J. G. Proakis and M. Salehi, *Digital Communications.* New York, NY, USA: McGraw-Hill, 2008.

[17] X. Yi, W. Shieh, and Y. Tang, "Phase estimation for coherent optical OFDM," *IEEE Photon. Technol. Lett.,* vol. 19, no. 12, pp. 919–921, Jun. 2007.

[18] S. L. Jansen, I. Morita, T. C. Schenk, and H. Tanaka, "Long-haul transmission of 16 × 52.5 Gbits/s polarization-division-multiplexed OFDM enabled by MIMO processing (Invited)," *J. Opt. Netw.,* no. 7, pp. 173–182, 2008.

[19] C. Pulikkaseril, L. A. Stewart, M. A. F. Roelens, G. W. Baxter, S. Poole, and S. Frisken, "Spectral modeling of channel band shapes in wavelength selective switches," *Opt. Exp.,* vol. 9, no. 19, pp. 8458–8470, 2011.